

Parameter dependence of the β -decay properties of neutron-rich Zr isotopes within the interacting boson model

M. Homma¹ and K. Nomura^{1,2,*}

¹*Department of Physics, Hokkaido University, Sapporo 060-0810, Japan*

²*Nuclear Reaction Data Center, Hokkaido University, Sapporo 060-0810, Japan*



(Received 20 April 2024; accepted 13 June 2024; published 1 July 2024)

We investigate parameter dependence of the calculated β -decay properties as well as low-lying states for the neutron-rich Zr isotopes within the neutron-proton interacting boson model (IBM-2) and interacting boson-fermion-fermion model (IBFFM-2). It is shown that the calculated $\log_{10} ft$ values for the transitions of the 0_1^+ ground states of the parent even-even nuclei $^{96-102}\text{Zr}$ into the 1_1^+ states of the daughter odd-odd nuclei $^{96-102}\text{Nb}$ consistently exhibit a strong dependence on those parameters associated with the quadrupole-quadrupole boson interaction, and with the residual interaction between an unpaired neutron and an unpaired proton in the IBFFM-2 Hamiltonian for the odd-odd Nb nuclei. By the reduction in magnitude of the quadrupole-quadrupole interaction strength by approximately a factor of 2, the calculated $\log_{10} ft$ values for the $\text{Zr}(0_1^+) \rightarrow \text{Nb}(1_1^+)$ transitions increase and agree with the experimental values. This points to a significant improvement over the previous study performed in the same mass region, that consists of the mapping from a relativistic energy density functional calculation onto the IBM-2 Hamiltonian.

DOI: [10.1103/PhysRevC.110.014303](https://doi.org/10.1103/PhysRevC.110.014303)

I. INTRODUCTION

Nuclear β -decay is a process in which a neutron in a nucleus is converted into a proton, or vice versa, emitting an electron (positron) and an antineutrino (electron neutrino). The β decay plays an essential role in the rapid neutron-capture processes in astrophysical nucleosynthesis, which produce heavy chemical elements, and is also used as an experimental technique to measure energy levels of a given nucleus. The β -decay rates of numerous neutron-rich heavy nuclei have been measured extensively by experiments in major radioactive-ion-beam facilities worldwide [1–5], which also calls for reliable theoretical predictions.

Accurate theoretical predictions as well as experimental measurements of the β decay also provide input to evaluate the double- β decay nuclear matrix elements [6–8]. It is a rare process in which, when the Q_β value of the single- β decay from the even-even to odd-odd nuclei is high enough, a decay process may occur between neighboring even-even nuclei with the neutron and proton numbers $(N, Z) = (N \mp 2, Z \pm 2)$, emitting two electrons (positrons) and some light particles. Theoretical evaluation of the double- β decay nuclear matrix elements currently differs by a factor of 2–3 among different nuclear models, and reduction of the theoretical uncertainty is under active investigation.

Precise calculations of the nuclear wave functions for the low-lying states of the initial and final nuclei, which enter the relevant transition operators, are crucial to provide reliable predictions of the β -decay properties, such as the half-lives and $\log_{10} ft$ values. Theoretical approaches that allow for the

calculation of the β -decay properties along with a quantitative and detailed description of the low-energy excitations have been made, e.g., by the nuclear shell model [9–12], quasiparticle random phase approximations [13–21], and the interacting boson model (IBM) [22–35].

In a recent article [35], a simultaneous description of the low-lying states and (allowed) β -decay properties of the neutron-rich even-even and odd-odd nuclei from the ^{36}Kr to ^{48}Cd isotopes near $N = 60$ was made by using the IBM that is based on the energy density functional (EDF) framework. In Ref. [35], the constrained self-consistent mean-field (SCMF) calculations were performed within the relativistic Hartree-Bogoliubov (RHB) model [36,37] using the density-dependent point-coupling (DD-PC1) EDF [38] and the separable pairing force of finite range [39]. The constrained calculations provided each even-even nucleus with the potential energy surface (PES) in terms of the triaxial quadrupole deformations, which is then mapped onto the expectation value of the neutron-proton IBM (IBM-2) Hamiltonian in the boson condensate state [40] for the even-even nuclei. This mapping procedure completely determines the parameters of the IBM-2 Hamiltonian. The same RHB SCMF calculation produced single-particle energies and occupation probabilities at spherical configuration for the neighboring odd-odd nuclei, and these quantities were used to determine the neutron-proton interacting boson-fermion-fermion model (IBFFM-2) [41,42] Hamiltonian for the odd-odd systems. Remaining coupling constants for the interactions between an odd neutron and an odd proton, and between an odd nucleon and even-even boson core were fit to reproduce a few low-lying states of each odd-odd nucleus to a reasonable accuracy. The Gamow-Teller (GT) transition strengths between an even-even and an odd-odd nuclei have been

*Contact author: nomura@sci.hokudai.ac.jp

computed by using those nuclear wave functions that were obtained from the IBM-2 and IBFFM-2 Hamiltonians, respectively, and were employed for calculating the β -decay $\log_{10} ft$ values.

It was found in Ref. [35], however, that the $\log_{10} ft$ values for the β^- decay of the studied even-even into odd-odd nuclei, especially for those of Kr, Sr, and Zr nuclei near $N = 60$ and $Z = 40$, are systematically underestimated by a factor of ≈ 1.5 within the mapped IBM-2 framework. These too small $\log_{10} ft$ values, hence too large GT transition matrix elements, imply some deficiencies of this method, which could be effectively accounted for by introducing certain amount of quenching of the axial-vector coupling constant g_A . The significant discrepancy between the experimental and calculated $\log_{10} ft$ values encountered in Ref. [35], however, would require one to use an unrealistically large quenching factor to reproduce the data. A possible cause of this discrepancy was also investigated in that study, and was attributed to the choice of the employed EDF that is a basis for determining most of the model parameters. Another possible factors that could give rise to the too small $\log_{10} ft$ values would lie in the IBM-2 and IBFFM-2 calculations, which provide nuclear wave functions for the parent and daughter nuclei.

In the present article, we report an extensive analysis of the dependence of the $\log_{10} ft$ predictions on various model parameters involved in the nuclear structure calculations within the IBM-2 and IBFFM-2, and attempt to identify which of the model parameters affect most significantly the final results on the $\log_{10} ft$ values. We show systematic behaviors of the calculated properties, such as the excitation energies for each parent and daughter nuclei, and the $\log_{10} ft$ values, as functions of a given model parameter. The present study is based on the previous work of Ref. [35], and hence the Hamiltonian parameters, and other ingredients, e.g., single-particle energies and occupation probabilities, that were obtained in the mapped IBM-2 calculations of Ref. [35] are here considered as a starting point for our analysis. In that way, we explore possible ways of improving the mapped IBM-2 description of β decay. We further calculate low-lying states of each of the parent and daughter nuclei to investigate how an optimal set of parameters that gives a reasonable agreement with the observed $\log_{10} ft$ values can reproduce the experimental energy spectrum in comparison to the previous calculation [35]. The parameter dependence of the excitation energies of odd-odd nuclei has been investigated within the IBFFM-2, e.g., in Ref. [34], but to the best of our knowledge the behaviors of the $\log_{10} ft$ values according to the IBFFM-2 parameters have not been studied.

Considering the fact that a large number of independent parameters enter the model, which in principle correlate with others and also differ from one nucleus to another, to keep the discussion as simple as possible we here focus on the β^- decay of the $^{96-102}\text{Zr}$ isotopes. The low-lying structure of the neutron-rich Zr isotopes has attracted considerable attention, since they exhibit a rapid shape transition at $N \approx 60$ and a possible shape coexistence [43]. ^{96}Zr is also a candidate nucleus for the two-neutrino and neutrinoless double- β decays, and its nuclear structural and single- β decay properties should be of much relevance.

The paper is structured as follows. In Sec. II we review the IBM-2 and IBFFM-2 Hamiltonians, their parameters, and GT transition operators, which were used in Ref. [35]. We show in Sec. III the parameter dependence of the $\log_{10} ft$ values on the model parameters. The variations with the parameters of the calculated excitation energies are discussed in Sec. IV. Section V gives a summary and perspectives for a future study.

II. THEORETICAL FRAMEWORK

This section gives a brief reminder of the IBM-2 and IBFFM-2 frameworks for calculating the β decay matrix elements. More detailed descriptions of these theoretical framework are found in Ref. [35] for the neutron-rich Zr region, and for general descriptions of the β -decay studies of odd-mass and odd-odd nuclei the reader is referred to Refs. [23,24,42] and [26,27], respectively.

A. Model Hamiltonian and GT operator

Within the IBM-2, an even-even core nucleus is described in terms of the neutron s_ν and d_ν bosons, and the proton s_π and d_π bosons [44]. From a microscopic point of view, the neutron (proton) s_ν and d_ν (s_π and d_π) bosons represent collective monopole and quadrupole pairs of valence neutrons (protons), respectively [44–46]. For the IBM-2 Hamiltonian we take the form

$$\hat{H}_B = \epsilon_d(\hat{n}_{d_\nu} + \hat{n}_{d_\pi}) + \kappa \hat{Q}_\nu \cdot \hat{Q}_\pi + \kappa_\nu \hat{Q}_\nu \cdot \hat{Q}_\nu + \kappa_\pi \hat{Q}_\pi \cdot \hat{Q}_\pi + \kappa' \hat{L} \cdot \hat{L}, \quad (1)$$

where the first term stands for the d -boson number operator with $\hat{n}_{d_\rho} = d_\rho^\dagger \cdot \tilde{d}_\rho$ ($\rho = \nu$ or π) and with ϵ_d the single d boson energy. The second, third, and fourth terms are the quadrupole-quadrupole interactions between neutron and proton bosons, between neutron and neutron bosons, and between proton and proton bosons, respectively. The quadrupole operator \hat{Q}_ρ is defined as $\hat{Q}_\rho = s_\rho^\dagger \tilde{d}_\rho + d_\rho^\dagger s_\rho + \chi_\rho (d_\rho^\dagger \times \tilde{d}_\rho)^{(2)}$, with χ_ν and χ_π being dimensionless parameters. κ , κ_ν , and κ_π are strength parameters. The fifth term in Eq. (1) stands for a rotational term, with κ' being the strength parameter, and $\hat{L} = \hat{L}_\nu + \hat{L}_\pi$ denotes the angular momentum operator with $\hat{L}_\rho = (d_\rho^\dagger \times \tilde{d}_\rho)^{(1)}$.

The IBM-2 is extended to treat odd-odd nuclear systems by including an unpaired neutron and an unpaired proton degrees of freedom, and their couplings. The IBFFM-2 Hamiltonian is expressed in general by

$$\hat{H} = \hat{H}_B + \hat{H}_F^\nu + \hat{H}_F^\pi + \hat{V}_{\text{BF}}^\nu + \hat{V}_{\text{BF}}^\pi + \hat{V}_{\nu\pi}. \quad (2)$$

The first term represents the IBM-2 core Hamiltonian (1). The second and third terms of Eq. (2) represent the single-neutron and -proton Hamiltonians, respectively, and take the form

$$\hat{H}_F^\rho = - \sum_{j_\rho} \epsilon_{j_\rho} \sqrt{2j_\rho + 1} (a_{j_\rho}^\dagger \times \tilde{a}_{j_\rho})^{(0)} \equiv \sum_{j_\rho} \epsilon_{j_\rho} \hat{n}_{j_\rho}, \quad (3)$$

where ϵ_{j_ρ} stands for the single-particle energy of the odd neutron or proton orbital j_ρ . $a_{j_\rho}^{(\dagger)}$ represents the particle annihilation (creation) operator, with \tilde{a}_{j_ρ} defined by $\tilde{a}_{j_\rho m_\rho} = (-1)^{j_\rho - m_\rho} a_{j_\rho - m_\rho}$. On the right-hand side of Eq. (3), \hat{n}_{j_ρ} stands for the number operator for the odd particle. The single-particle space taken in the present study comprises

the neutron $3s_{1/2}$, $2d_{3/2}$, $2d_{5/2}$, and $1g_{7/2}$ orbitals, and the proton $1g_{9/2}$ orbital in the $N = 50$ – 82 and $Z = 28$ – 50 major oscillator shells for calculating the positive-parity states of the odd-odd Nb nuclei. For $^{96-102}\text{Nb}$, since the odd neutron and odd proton are, respectively, treated as a particle and a hole, the corresponding even-even boson cores are the $^{96-102}\text{Mo}$ nuclei, respectively.

The fourth (fifth) term on the right-hand side of Eq. (2) denotes the interaction between a single neutron (or proton)

$$\hat{V}_{\text{dyn}}^{\rho} = \sum_{j_{\rho} j'_{\rho}} \gamma_{j_{\rho} j'_{\rho}} (a_{j_{\rho}}^{\dagger} \times \tilde{a}_{j'_{\rho}})^{(2)} \cdot \hat{Q}_{\rho'}, \quad (5)$$

$$\hat{V}_{\text{exc}}^{\rho} = -(s_{\rho'}^{\dagger} \times \tilde{d}_{\rho'})^{(2)} \cdot \sum_{j_{\rho} j'_{\rho} j''_{\rho}} \sqrt{\frac{10}{N_{\rho}(2j_{\rho} + 1)}} \beta_{j_{\rho} j'_{\rho}} \beta_{j''_{\rho} j_{\rho}} : [(d_{\rho}^{\dagger} \times \tilde{a}_{j''_{\rho}})^{(j_{\rho})} \times (a_{j'_{\rho}}^{\dagger} \times \tilde{s}_{\rho})^{(j'_{\rho})}]^{(2)} : + (\text{H.c.}), \quad (6)$$

$$\hat{V}_{\text{mon}}^{\rho} = \hat{n}_{d_{\rho}} \hat{n}_{j_{\rho}}, \quad (7)$$

where the j -dependent factors $\gamma_{j_{\rho} j'_{\rho}} = (u_{j_{\rho}} u_{j'_{\rho}} - v_{j_{\rho}} v_{j'_{\rho}}) Q_{j_{\rho} j'_{\rho}}$, and $\beta_{j_{\rho} j'_{\rho}} = (u_{j_{\rho}} v_{j'_{\rho}} + v_{j_{\rho}} u_{j'_{\rho}}) Q_{j_{\rho} j'_{\rho}}$, with $Q_{j_{\rho} j'_{\rho}} = \langle \ell_{\rho} \frac{1}{2} j_{\rho} \| Y^{(2)} \| \ell'_{\rho} \frac{1}{2} j'_{\rho} \rangle$ being the matrix element of the fermion quadrupole operator in the single-particle basis. $\hat{Q}_{\rho'}$ in Eq. (5) denotes the quadrupole operator in the boson system, introduced in Eq. (1). The notation $:(\dots):$ in Eq. (6) stands for normal ordering. Note that the forms of $\hat{V}_{\text{BF}}^{\rho}$ have been discussed on microscopic grounds in Refs. [42,47]. Within this framework the unperturbed single-particle energy, $\epsilon_{j_{\rho}}$, in Eq. (3) should be replaced with the quasiparticle energy $\tilde{\epsilon}_{j_{\rho}}$.

The last term of Eq. (2), $\hat{V}_{v\pi}$, corresponds to the residual interaction between the unpaired neutron and proton. The following form is here considered for this interaction:

$$\hat{V}_{v\pi} = 4\pi v_d \delta(\mathbf{r}) \delta(\mathbf{r}_v - \mathbf{r}_0) \delta(\mathbf{r}_{\pi} - \mathbf{r}_0) + v_t \left[\frac{3(\boldsymbol{\sigma}_v \cdot \mathbf{r})(\boldsymbol{\sigma}_{\pi} \cdot \mathbf{r})}{r^2} - \boldsymbol{\sigma}_v \cdot \boldsymbol{\sigma}_{\pi} \right]. \quad (8)$$

The first and second terms stand for the δ and tensor interactions, with v_d , and v_t being strength parameters, respectively. Note that $\mathbf{r} = \mathbf{r}_v - \mathbf{r}_{\pi}$ is the relative coordinate of the neutron and proton, and $r_0 = 1.2A^{1/3}$ fm. The matrix element of $\hat{V}_{v\pi}$ depends on the occupation v_j and unoccupation u_j amplitudes.

The GT transition operator is here defined by

$$\hat{T}^{\text{GT}} = \sum_{j_{\nu} j_{\pi}} \eta_{j_{\nu} j_{\pi}}^{\text{GT}} (\hat{P}_{j_{\nu}} \times \hat{P}_{j_{\pi}})^{(1)}, \quad (9)$$

with the coefficients η calculated as

$$\eta_{j_{\nu} j_{\pi}}^{\text{GT}} = -\frac{1}{\sqrt{3}} \left\langle \ell_{\nu} \frac{1}{2} j_{\nu} \left\| \boldsymbol{\sigma} \left\| \ell_{\pi} \frac{1}{2} j_{\pi} \right. \right. \right\rangle \delta_{\ell_{\nu} \ell_{\pi}}. \quad (10)$$

$\hat{P}_{j_{\nu}}$ and $\hat{P}_{j_{\pi}}$ in Eq. (9) are one-particle transfer operators, expressed as

$$\hat{P}_{j_{\nu}} = \zeta_{j_{\nu}}^* \tilde{a}_{j_{\nu} m_{j_{\nu}}} + \sum_{j'_{\nu}} \zeta_{j_{\nu} j'_{\nu}}^* s_{\nu} (d_{\nu}^{\dagger} \times \tilde{a}_{j'_{\nu}})_{m_{j_{\nu}}}^{(j_{\nu})}, \quad (11)$$

$$\hat{P}_{j_{\pi}} = -\theta_{j_{\pi}}^* s_{\pi} a_{j_{\pi} m_{j_{\pi}}}^{\dagger} - \sum_{j'_{\pi}} \theta_{j_{\pi} j'_{\pi}}^* (\tilde{d}_{\pi} \times a_{j'_{\pi}}^{\dagger})_{m_{j_{\pi}}}^{(j_{\pi})}, \quad (12)$$

and the even-even boson core, and is given as [42,47]

$$\hat{V}_{\text{BF}}^{\rho} = \Gamma_{\rho} \hat{V}_{\text{dyn}}^{\rho} + \Lambda_{\rho} \hat{V}_{\text{exc}}^{\rho} + A_{\rho} \hat{V}_{\text{mon}}^{\rho}, \quad (4)$$

where the first, second, and third terms represent the quadrupole dynamical, exchange, and monopole interactions, respectively, with the strength parameters Γ_{ρ} , Λ_{ρ} , and A_{ρ} . Each term in the above expression reads

for the β^{-} decay of the Zr isotopes. The operators in Eqs. (11) and (12), respectively, increase and decrease the number of like-hole nucleons, and both of them decrease the valence nucleon number by 1. The coefficients ζ_j , $\zeta_{jj'}$, θ_j , and $\theta_{jj'}$ in Eqs. (11) and (12) are calculated within the generalized seniority scheme [23], and depend on the u_j and v_j amplitudes. Their explicit forms are found in Ref. [35].

The ft values in seconds are obtained via the calculated GT matrix element between the initial I_i state of the parent nucleus and the final I_f state of the daughter nucleus, $M_{\text{GT}} = \langle I_f \| \hat{T}^{\text{GT}} \| I_i \rangle$, i.e.,

$$ft = \frac{6163}{(g_A/g_V)^2 |M_{\text{GT}}|^2}, \quad (13)$$

with $g_A = 1.27$ and $g_V = 1$ being the axial-vector and vector coupling constants, respectively.

B. Summary of the model parameters

The parameters for the IBM-2 Hamiltonian involved in the present study are ϵ_d , κ , κ_{ν} , κ_{π} , χ_{ν} , χ_{π} , and κ' . To reduce the number of parameters, as in the previous study [35], a simplification is made on the strength parameters for the different quadrupole-quadrupole boson interactions, so that $\kappa_{\nu} = \kappa_{\pi} = \kappa/2$ for the even-even $^{96-102}\text{Zr}$ nuclei and $\kappa_{\nu} = \kappa_{\pi} = 0$ for the even-even $^{96-102}\text{Mo}$ nuclei, which are taken as the boson cores for the odd-odd $^{96-102}\text{Nb}$ nuclei. In addition, in Ref. [35] the $\hat{L} \cdot \hat{L}$ term was included in the IBM-2 Hamiltonian for the even-even Zr nuclei, but was not for the even-even Mo nuclei. In a number of microscopic [46,48,49] and phenomenological [44] IBM-2 calculations carried out to date, however, it has been shown that a simplified form of the Hamiltonian consisting of the \hat{n}_d , and $\hat{Q}_{\nu} \cdot \hat{Q}_{\pi}$ terms describes the low-energy quadrupole collective states of most of the medium-heavy and heavy nuclei. Thus, in the following we regard the parameters ϵ_d , κ , χ_{ν} , and χ_{π} the most relevant parameters among the IBM-2 Hamiltonian (1), and investigate dependencies of the results on these parameters, concerning the bosonic interactions. Tables I and II summarize, respectively, the IBM-2

TABLE I. The IBM-2 parameters for the parent nuclei $^{96-102}\text{Zr}$ used in Ref. [35], which have been obtained from mapping the RHB SCMF onto the IBM-2 deformation energy surfaces. Note that the like-boson quadrupole-quadrupole interaction strengths are assumed to take the values $\kappa_{\nu,i} = \kappa_{\pi,i} = \kappa_i/2$.

Nucleus	$\epsilon_{d,i}$ (MeV)	κ_i (MeV)	$\chi_{\nu,i}$	$\chi_{\pi,i}$	κ'_i (MeV)
^{96}Zr	0.34	-0.18	-0.35	0.24	0.051
^{98}Zr	0.28	-0.15	-0.54	0.11	0.032
^{100}Zr	0.036	-0.094	-0.45	0.20	0.0020
^{102}Zr	0.081	-0.081	-0.52	0.49	0.0037

parameters for the even-even $^{96-102}\text{Zr}$ and odd-odd $^{96-102}\text{Nb}$ nuclei. They were determined microscopically by mapping the RHB PES onto the corresponding IBM-2 one in Ref. [35]. To avoid confusion, we express from now on those IBM-2 parameters used for the parent Zr nuclei by putting a subscript “ i ”, representing the initial state, and those for the daughter Nb nuclei with a subscript “ f ”, so as to represent the final state.

Six parameters in the IBFFM-2 Hamiltonian, Γ_ν , Λ_ν , A_ν , Γ_π , Λ_π , and A_π , which are the coefficients of the boson-fermion interactions, are here treated as free parameters, and the variations of the results with these parameters are investigated. The quasiparticle energies $\tilde{\epsilon}_{j\rho}$ in \hat{H}_F , and occupation probabilities $v_{j\rho}^2$, which appear in \hat{V}_{BF} and GT operator, are kept constant so as to be the same values as those used in the previous study of Ref. [35]. The parameters v_d , and v_t in the residual interaction $\hat{V}_{\nu\pi}$ are additional variable parameters. Those v_d and v_t values employed in Ref. [35] are summarized in Table III.

III. IMPACTS ON THE β -DECAY PROPERTIES

A. $\log_{10} ft$ values

Figures 1–5 show the calculated $\log_{10} ft$ values for the β^- decay of the 0_1^+ ground state of the even-even $^{96-102}\text{Zr}$ nuclei into the lowest four 1^+ states of the odd-odd $^{96-102}\text{Nb}$ nuclei as functions of the following model parameters: the IBM-2 parameters in the parent Zr nuclei (Fig. 1), the parameters for the even-even boson cores (Fig. 2), strength parameters for the interactions between the odd neutron and boson core (Fig. 3) and between the odd proton and boson core (Fig. 4), and strength parameters v_d and v_t for the residual neutron-proton interaction (Fig. 5) for the odd-odd daughter nuclei Nb.

TABLE II. The boson-core parameters for the odd-odd daughter nuclei $^{96-102}\text{Nb}$ used in Ref. [35]. Note that the strength parameters $\kappa_{\pi,i} = \kappa_{\pi,f} = 0$ MeV and $\kappa'_f = 0$ MeV.

Nucleus	$\epsilon_{d,f}$ (MeV)	κ_f (MeV)	$\chi_{\nu,f}$	$\chi_{\pi,f}$
^{96}Nb	0.69	-0.44	-0.65	0.45
^{98}Nb	0.95	-0.41	-0.57	0.08
^{100}Nb	0.58	-0.35	-0.50	0.45
^{102}Nb	0.52	-0.27	-0.43	0.36

TABLE III. Adopted strength parameters (in MeV units) for the boson-fermion interactions, and fermion-fermion interactions in the IBFFM-2 Hamiltonian describing the odd-odd $^{96-102}\text{Nb}$ nuclei. The fixed value, $v_d = -0.08$ MeV, is employed for the δ term. The spin-spin interaction strength, $v_{ss} = 0.1$ MeV is used specifically for ^{96}Nb .

Nucleus	Γ_ν	Γ_π	Λ_ν	Λ_π	A_ν	A_π	v_t
^{96}Nb	0.30	0.30	0.40	0.90	-0.00	-0.50	0
^{98}Nb	1.50	0.10	0.80	0.00	-1.20	-0.00	0.280
^{100}Nb	1.50	0.30	0.50	0.20	-1.40	-0.80	0.500
^{102}Nb	1.50	0.10	0.90	3.80	-0.90	-2.00	0.500

One can see from Fig. 1 that the $\log_{10} ft(0_1^+ \rightarrow 1_{1,2}^+)$ values do not depend much on all the IBM-2 parameters in the parent Zr nuclei. The calculated values $\log_{10} ft(0_1^+ \rightarrow 1_1^+) \approx 3.5$ do not differ from the ones obtained from the mapped IBM-2 parameter (represented by the vertical dotted line in each panel), and are also much below the observed $\log_{10} ft$ values [50] (horizontal dashed lines): 4.154, 4.6, and 4.71 for the $^{98}\text{Zr}(0_1^+) \rightarrow ^{98}\text{Nb}(1_1^+)$, $^{100}\text{Zr}(0_1^+) \rightarrow ^{100}\text{Nb}(1_1^+)$, and $^{102}\text{Zr}(0_1^+) \rightarrow ^{102}\text{Nb}(1_1^+)$ decays, respectively. Note that the $\log_{10} ft$ data are not available for the $^{96}\text{Zr}(0_1^+) \rightarrow ^{96}\text{Nb}(1_1^+)$ decay. The $\log_{10} ft(0_1^+ \rightarrow 1_{3,4}^+)$ values seem to be more sensitive to the IBM-2 parameters for the parent nuclei.

One should notice that, at some specific values of the IBM-2 parameters, the calculated $\log_{10} ft$'s are extremely large, as observed, for instance, in the $^{96}\text{Zr}(0_1^+) \rightarrow ^{96}\text{Nb}(1_3^+) \beta^-$ decay at $\epsilon_{d,i} \approx 0.1$ MeV. The spike-like pattern or discontinuity in $\log_{10} ft$ could be explained by the fact that, with a particular combination of the parameters, matrix elements for different components in the GT operator happen to cancel each other to such an extent that the resultant M_{GT} matrix element nearly vanishes, hence the extremely large $\log_{10} ft$ value is obtained. The cancellation of this sort seems to occur rather accidentally mainly for the β^- decays to higher lying non-yrast 1^+ states. These are, all in all, local behaviors typically found at higher 1^+ excitation energies, but do not appear in most of the $\log_{10} ft(0_1^+ \rightarrow 1_1^+)$ systematic. In addition, as we show in Sec. III B, they also do not make any sizable contribution to the entire GT strength distributions and their running sums involving a number of 1^+ states of the odd-odd Nb nuclei. Therefore we consider the spike-like patterns of $\log_{10} ft$'s at higher 1^+ states to be rather unimportant in the present analysis, especially since we intend to optimize parameters by using the $\log_{10} ft$ data for the lowest-energy, 1_1^+ state.

In comparison to the behaviors of the $\log_{10} ft$ values as functions of the IBM-2 parameters for the parent even-even nuclei, one may notice in Fig. 2 that the calculated $\log_{10} ft$ values are rather sensitive to the boson-core Hamiltonian parameters for the odd-odd Nb nuclei. What is particularly worth noting is the fact that the $\log_{10} ft$ values for the $^{98,100,102}\text{Zr}(0_1^+) \rightarrow ^{98,100,102}\text{Nb}(1_1^+)$ decays substantially increase with the parameter κ_f , in the range $\kappa_f \gtrsim -0.2$ MeV. A similar $\log_{10} ft$ systematic is present for the $^{96}\text{Zr}(0_1^+) \rightarrow ^{96}\text{Nb}(1_1^+)$ decay as well for the region of even smaller $|\kappa_f|$ values, $\kappa_f \gtrsim -0.1$. Similarly, the $^A\text{Zr}(0_1^+) \rightarrow ^A\text{Nb}(1_1^+)$ decay $\log_{10} ft$ values with $A = 98$ and 100 increase with the parameter κ_i used for the parent Zr nuclei (see Fig. 1). The

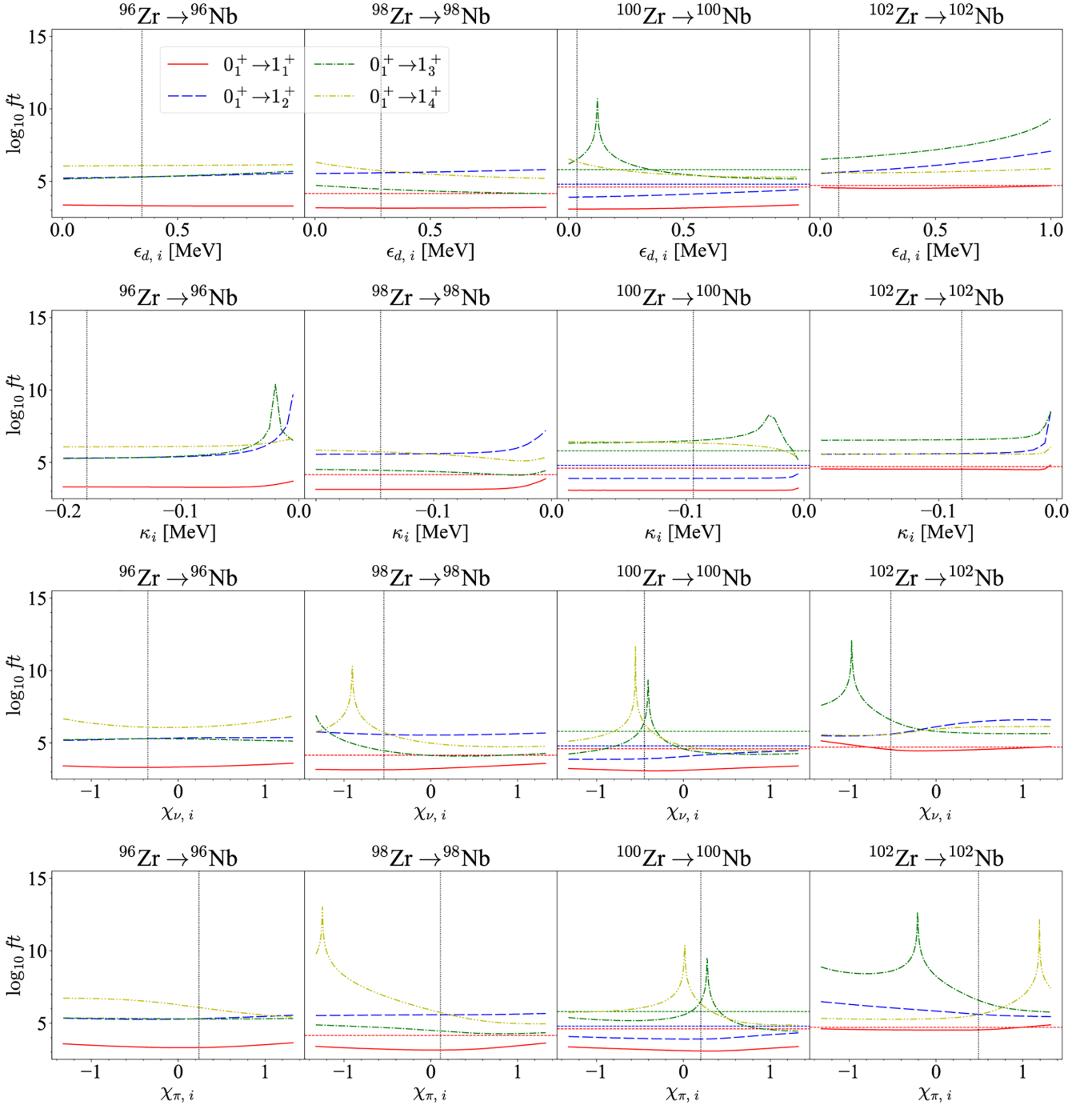


FIG. 1. Variations of the calculated $\log_{10} ft$ values for the β^- decays of the 0_1^+ ground states of the even-even $^{96-104}\text{Zr}$ nuclei into the lowest four 1^+ states of the odd-odd $^{96-102}\text{Nb}$ nuclei as functions of the IBM-2 parameters for the parent Zr nuclei. The vertical dotted line in each panel indicates the value of the parameter obtained from the RHB-to-IBM mapping procedure. Available experimental $\log_{10} ft$ values are also indicated by horizontal dashed lines with the same colors used for the corresponding calculated values.

increase, however, occurs rather in a narrow region of κ_i , i.e., $\kappa_i \gtrsim -0.01$ MeV, which is almost vanishing, and so does not make much sense for a realistic calculation. One could also extract optimal values for the parameter κ_f , which result in agreement with the experimental $\log_{10} ft(0_1^+ \rightarrow 1_1^+)$, when available. For those $^A\text{Zr}(0_1^+) \rightarrow ^A\text{Nb}(1_1^+)$ decays with $A = 98, 100$, and 102 , the κ_f values of approximately -0.180 , -0.150 , and -0.260 MeV give a good description of the

corresponding $\log_{10} ft$ data. The above values correspond to the reduction in magnitude of $\approx 55\%$ of those adopted in the mapped IBM-2 calculations [35]. The calculated $\log_{10} ft$ values do not show a significant dependence on the parameters $\chi_{\nu,f}$ and $\chi_{\pi,f}$, an exception being perhaps the $^{102}\text{Zr}(0_1^+) \rightarrow ^{102}\text{Nb}(1_1^+)$ decay.

We notice in Fig. 3 that the predicted $\log_{10} ft(0_1^+ \rightarrow 1_1^+)$ values as a function of Γ_ν (the dynamical quadrupole

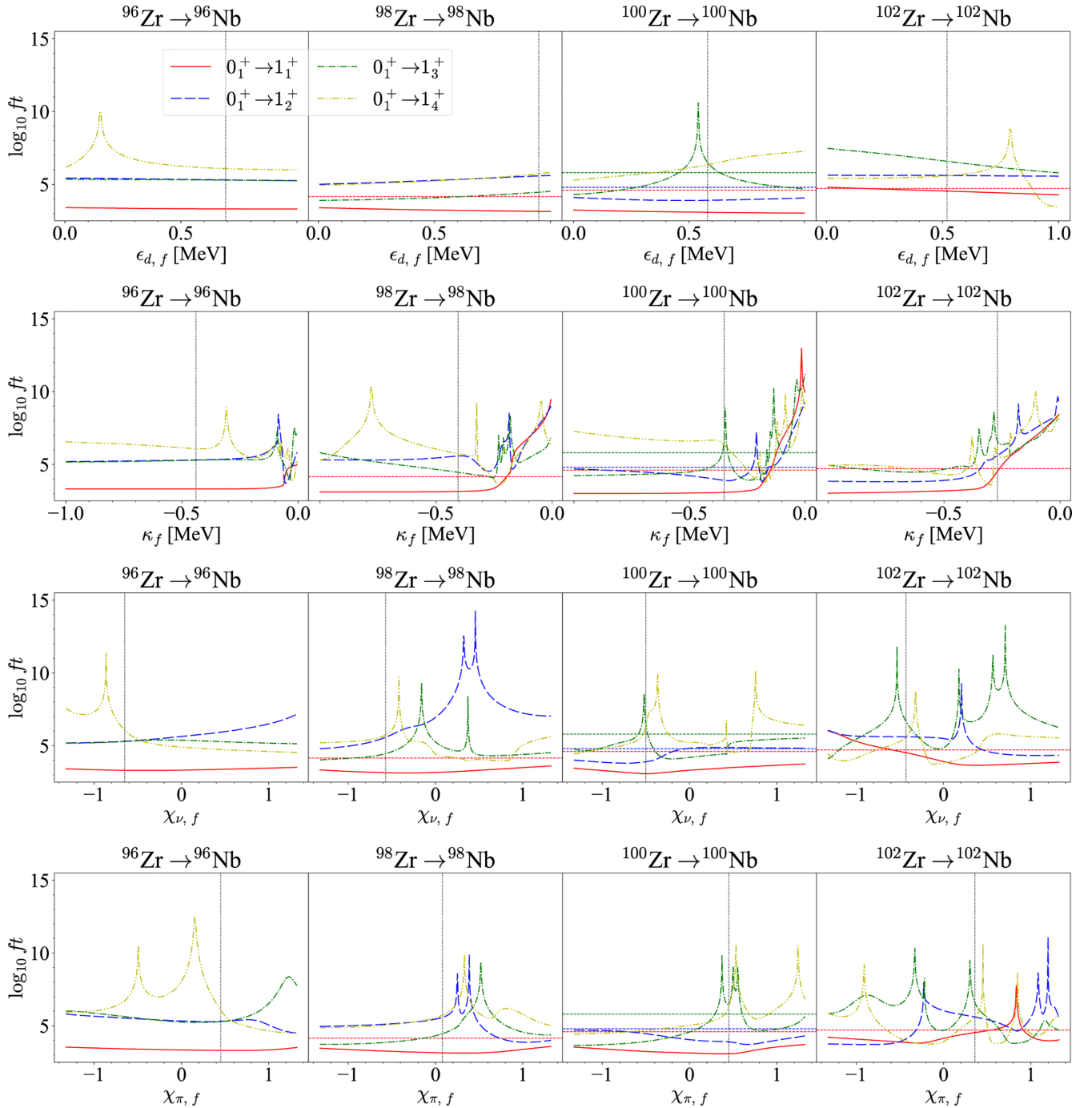


FIG. 2. Same as Fig. 1, but as functions of the boson-core parameters for the odd-odd daughter Nb nuclei.

interaction strength between the odd neutron and even-even boson core) are stable for most of the nuclei. A stronger parameter dependence of the ft values is seen in their evolution with the exchange interaction strength Λ_ν for the ${}^A\text{Zr}(0_1^+) \rightarrow {}^A\text{Nb}(1_1^+)$ decay with $A = 98, 100$, and 102 . It is worth noting that the exchange interaction reflects the fact that the bosons are made of pairs of fermions, and this type of the interaction has been shown to play an important role in reproducing low-energy levels of odd nuclei. It appears from the systematic shown in Fig. 3 that the exchange interaction also has

an impact on the calculation of the β -decay $\log_{10} ft$ values for $A = 98, 100$, and 102 , as well as the low-lying states. The monopole interaction strength A_ν does not seem to have an influence on the $\log_{10} ft$ calculations. It is more or less expected from the fact that this interaction only has an effect of either compressing or stretching a whole energy spectrum, and hence plays a less important role than the dynamical and exchange interactions. An exception is an irregular, spike-like, behavior of $\log_{10} ft(0_1^+ \rightarrow 1_1^+)$ at $A_\nu \approx -2$ MeV and ≈ 1.75 MeV in the case of the ${}^{102}\text{Zr} \rightarrow {}^{102}\text{Nb}$ decay.

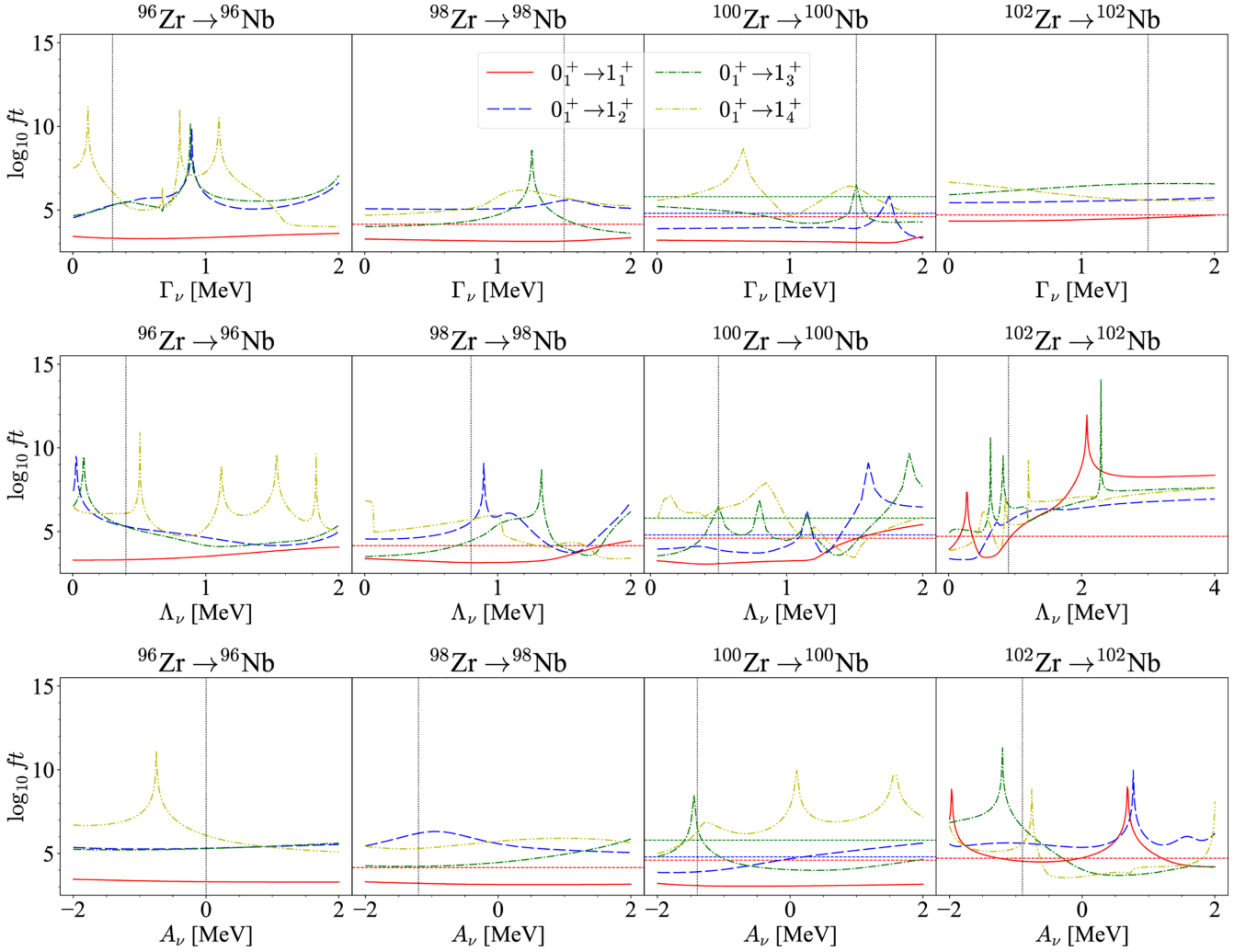


FIG. 3. Same as Fig. 1, but as functions of the interaction strengths between the odd neutron and even-even boson core for the odd-odd Nb nuclei.

It appears from Fig. 4 that the $\log_{10} ft$ values are less sensitive to Γ_π (the strength parameters for the interaction between the odd proton and even-even boson core), as the $\log_{10} ft(0_1^+ \rightarrow 1_1^+)$ value is almost constant against the variations of the Γ_π , Λ_π , and A_π parameters for most of the considered decay processes ${}^A\text{Zr} \rightarrow {}^A\text{Nb}$ with $A = 96, 98$, and 100 . One notices a certain dependence of the ${}^{102}\text{Zr}(0_1^+) \rightarrow {}^{102}\text{Nb}(1_1^+)$ $\log_{10} ft$ value on Λ_π , as it smoothly increases with $\Lambda_\pi \gtrsim 1$ MeV.

In Fig. 5, we observe a strong dependence of the ${}^{96}\text{Zr}(0_1^+) \rightarrow {}^{96}\text{Nb}(1_n^+)$ ($n = 1-4$) decay $\log_{10} ft$ values on the parameter v_d , a residual neutron-proton interaction strength of surface- δ type, seen most spectacularly in the sharp rise of the $\log_{10} ft(0_1^+ \rightarrow 1_1^+)$ value near $v_d = 0.2$ MeV. For the ${}^{98,100}\text{Zr}(0_1^+) \rightarrow {}^{98,100}\text{Nb}(1_n^+)$ decays, in contrast, the corresponding $\log_{10} ft$ values exhibit a much weaker dependence on v_d . The ${}^{102}\text{Zr}(0_1^+) \rightarrow {}^{102}\text{Nb}(1_{1,2}^+)$ decay $\log_{10} ft$ values show a decreasing pattern as functions of v_d , but the change is smooth and monotonic, as compared to the case of the ${}^{96}\text{Zr}(0_1^+) \rightarrow {}^{96}\text{Nb}(1_{1,2}^+)$ decay $\log_{10} ft$ values. Such a specialty for the ${}^{96}\text{Zr}(0_1^+) \rightarrow {}^{96}\text{Nb}(1_n^+)$ decays is perhaps due

to the fact that among the odd-odd Nb nuclei studied here only ${}^{96}\text{Nb}$ has the ground state with spin and parity $I^\pi = 6^+$, while the others have $I^\pi = 1^+$; to reproduce the 6^+ ground state, in Ref. [35] a different form of the residual neutron-proton interactions was considered for ${}^{96}\text{Nb}$, so that $v_t = 0$ MeV and a spin-spin interaction of the form $-\sigma_v \cdot \sigma_\pi / \sqrt{3}$ was specifically included for this nucleus (see Ref. [35] and the caption to Table III). As is clear from Fig. 5, the predicted $\log_{10} ft$ values, particular for the ${}^A\text{Zr}(0_1^+) \rightarrow {}^A\text{Nb}(1_{1,2}^+)$ decays of all the masses $A = 96-102$, consistently exhibit a strong dependence on v_t , in such a way that they rise sharply, as v_t decreases for $v_t < 0$. For the ${}^{98,100}\text{Zr}(0_1^+) \rightarrow {}^{98,100}\text{Nb}(1_1^+)$ decays, the value $v_t \approx -0.1 (< 0)$ MeV appears to lead to a good agreement with the experimental data, $\log_{10} ft \approx 4.154$ and 4.6 , respectively. Concerning the ${}^{102}\text{Zr}(0_1^+) \rightarrow {}^{102}\text{Nb}(1_1^+)$ decay, as it is seen from Fig. 5 the derived $v_t = 0.5$ MeV in the mapped IBM-2 framework already gives a reasonable agreement with the experimental value of $\log_{10} ft = 4.71$.

So far we have seen that the $\log_{10} ft(0_1^+ \rightarrow 1_1^+)$ values for the considered ${}^A\text{Zr} \rightarrow {}^A\text{Nb}$ β^- decays with $A = 96-102$ all show a particularly strong dependence on the parameters

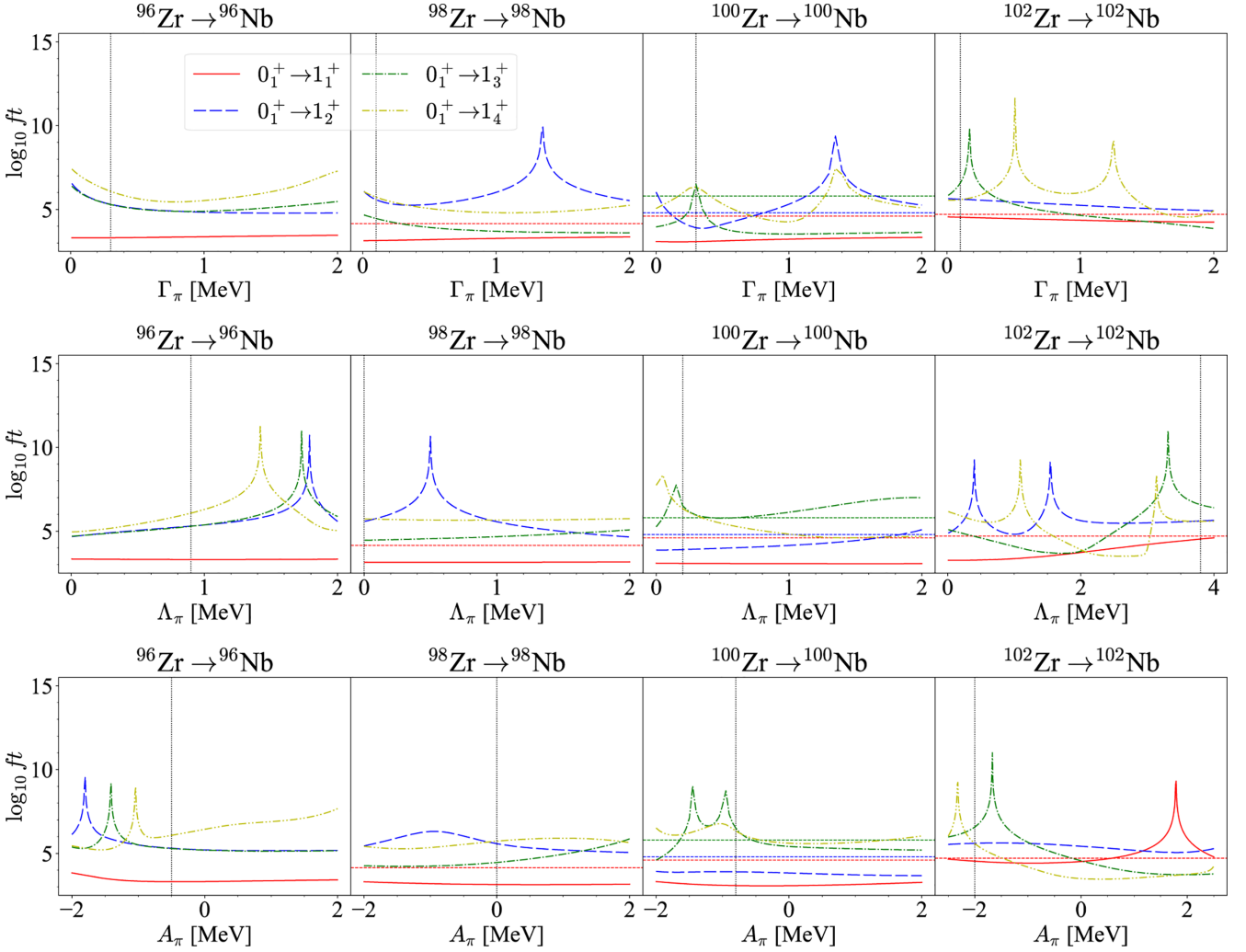


FIG. 4. Same as Fig. 1, but as functions of the interaction strengths between the odd proton and even-even boson core for the odd-odd Nb nuclei.

κ_f and v_t . We thus analyze the behaviors of the ${}^A\text{Zr}(0_1^+) \rightarrow {}^A\text{Nb}(1_1^+)$ decay $\log_{10} ft$ values when we change κ_f and v_t simultaneously. The results are presented in Fig. 6, where the calculated $\log_{10} ft(0_1^+ \rightarrow 1_1^+)$ values are depicted in contour plots. In the figure, the ${}^{96}\text{Zr}(0_1^+) \rightarrow {}^{96}\text{Nb}(1_1^+)$ decay $\log_{10} ft$ looks almost constant against κ_f , since only in the vicinity of $\kappa_f = 0$ MeV is a slight increase observed for $v_t > 0$ and some weak dependence on κ_f within the range $-0.6 \lesssim \kappa_f \lesssim -0.1$ MeV. When it is seen as a function of v_t , there appears a sharp decrease when it changes sign from $v_t < 0$ to $v_t > 0$. The β^- decays of the ${}^{98,100,102}\text{Zr}$ nuclei are more interesting here, since there are experimental $\log_{10} ft(0_1^+ \rightarrow 1_1^+)$ data available. As compared to the ${}^{96}\text{Zr}(0_1^+) \rightarrow {}^{96}\text{Nb}(1_1^+)$ decay $\log_{10} ft$ value, those for the ${}^{98,100,102}\text{Zr}(0_1^+) \rightarrow {}^{98,100,102}\text{Nb}(1_1^+)$ decays show a notable dependence on both the κ_f and v_t parameters. The predicted $\log_{10} ft(0_1^+ \rightarrow 1_1^+)$ values obtained from the RHB mapped-IBM-2 calculation [35], are shown as the crossing point of the vertical and horizontal dotted lines in each panel of Fig. 6, representing, respectively, those κ_f and v_t parameters employed in that calculation. We notice that they are rather far

from the observed $\log_{10} ft$ values, 4.154, 4.6, and 4.71 for the ${}^{98,100,102}\text{Zr}(0_1^+) \rightarrow {}^{98,100,102}\text{Nb}(1_1^+)$ decays, respectively. Based on the (κ_f, v_t) surfaces in Fig. 6, we can extract optimal sets of the κ_f and v_t values to improve description of the $\log_{10} ft$ data available for the ${}^{98,100,102}\text{Zr}$ β^- decays. For the ${}^A\text{Zr}(0_1^+) \rightarrow {}^A\text{Nb}(1_1^+)$ decays with $A = 98, 100$, and 102 , one could choose $\kappa_f = -0.180, -0.150$, and -0.260 MeV, respectively. Given these κ_f values, the $\log_{10} ft(0_1^+ \rightarrow 1_1^+)$ appears to be rather insensitive to v_t in the (κ_f, v_t) surface, so it would be just enough to employ the same v_t values as those used in the mapped IBM-2 calculations, i.e., $v_t = 0.28, 0.5$, and 0.5 MeV for the ${}^{98}\text{Zr}, {}^{100}\text{Zr}$, and ${}^{102}\text{Zr}$ β^- decays, respectively (cf. Table III).

B. GT strength distributions

Figure 7 displays absolute squares of the calculated GT transition matrix elements, $|M_{GT}(0_1^+ \rightarrow 1_n^+)|^2$, for the β^- decays of the even-even ${}^{96-102}\text{Zr}$ into odd-odd ${}^{98-102}\text{Nb}$ nuclei as functions of the excitation energies $E_x(1_n^+)$ of all the 1^+ states of the odd-odd daughter (Nb) nuclei, obtained from the IBFFM-2 Hamiltonian in the considered model space. The

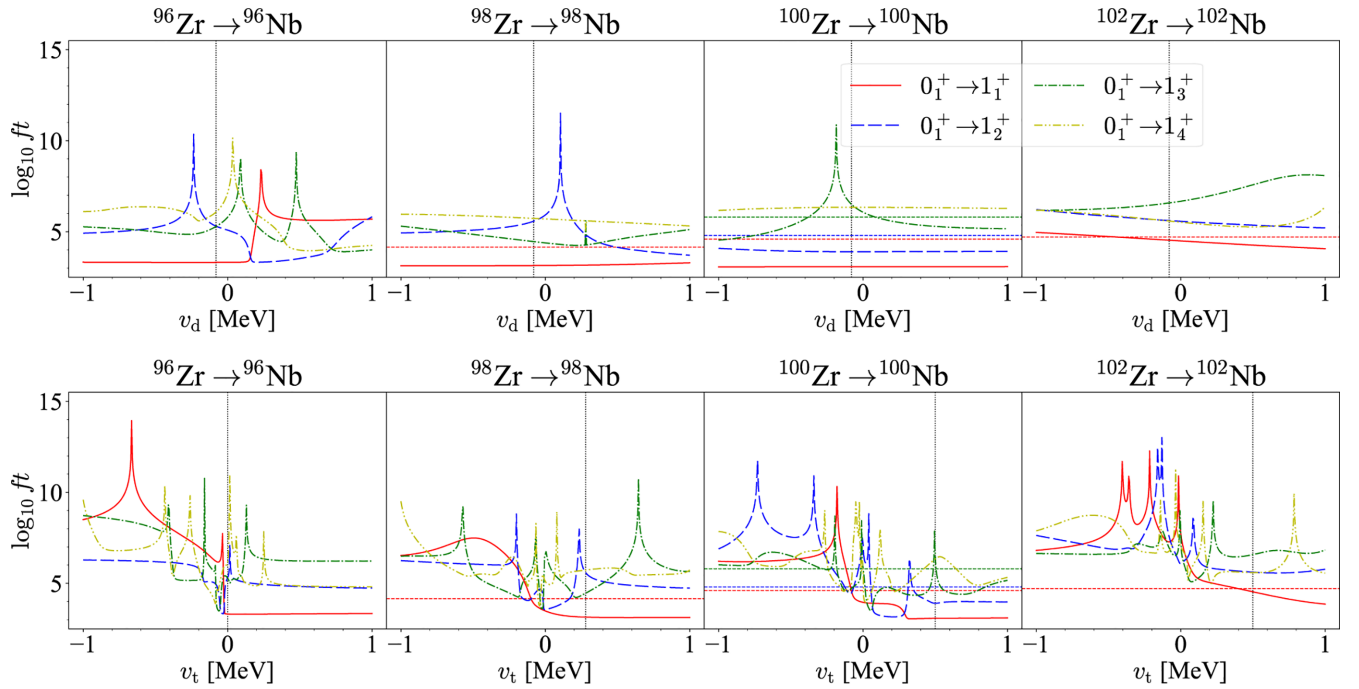


FIG. 5. Same as Fig. 1, but as functions of the strengths parameters for the residual neutron-proton interactions considered for the odd-odd Nb nuclei.

calculated results employing different values of the strength parameter κ_f for the odd-odd Nb nuclei are compared: the derived value from the RHB-to-IBM mapping in Ref. [35] (left column), and the optimal value extracted in the present work, that gives an agreement with the measured $\log_{10} ft(0_1^+ \rightarrow 1_1^+)$ (middle column). Also included on the right column of Fig. 7

are the results obtained with the κ_f values that give rise the “spike” pattern we observe in Fig. 2 in the calculated $\log_{10} ft$ values for non-yrast 1_1^+ states. Specifically, at the values $\kappa_f = -0.780$, -0.210 , and -0.380 MeV, the calculated $\log_{10} ft(0_1^+ \rightarrow 1_4^+)$, $\log_{10} ft(0_1^+ \rightarrow 1_3^+)$, and $\log_{10} ft(0_1^+ \rightarrow 1_2^+)$ values for the β^- decays of $^{98,100,102}\text{Zr}$, respectively, are extremely large (see Fig. 2).

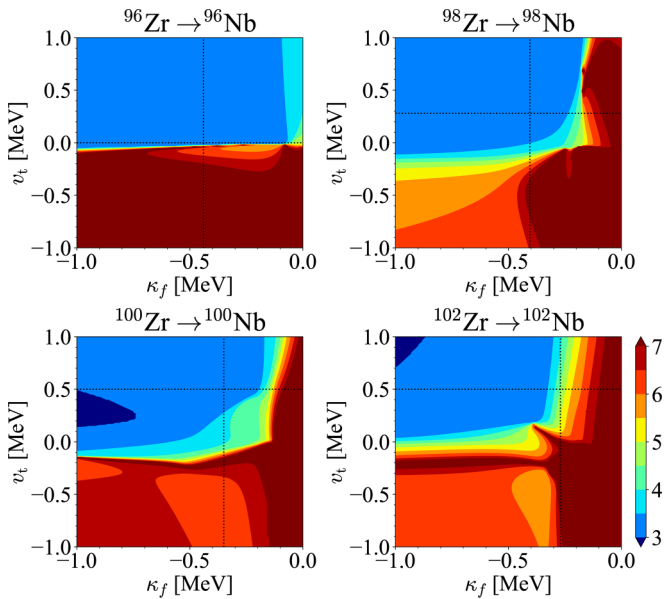


FIG. 6. Contour plots of the calculated β^- -decay $\log_{10} ft(0_1^+ \rightarrow 1_1^+)$ values for the even-even $^{96-102}\text{Zr}$ in terms of the parameters κ_f and v_t used for the odd-odd Nb nuclei. The vertical and horizontal dotted lines in each panel indicate those κ_f and v_t values employed in the mapped IBM-2 calculation of Ref. [35].

Note that the mapped IBM-2 results for the M_{GT} distributions were already presented in Fig. 9 of Ref. [35]. In that reference, the maximal number of iterations in the numerical diagonalization of the IBFFM-2 Hamiltonian using the Lanczos method were set to be 20000, 200 000, and 200, for ^{98}Nb , ^{100}Nb , and ^{102}Nb nuclei, respectively. In the present study, the iterations are carried out 200 000 times for all the Nb nuclei considered to achieve a better convergence. There is no noticeable difference between the previous result using the smaller number of the iterations, and the present one in the systematic of the GT transition distributions. An exception is the behaviors of the GT strengths for the high 1_1^+ excitation energies, which, however, only make negligible contributions to the gross feature of the M_{GT} distributions and their running sums.

It is seen from Fig. 7 that, in general, the GT transitions to low-lying 1_1^+ states below $E_x(1_1^+) \approx 1$ MeV make the dominant contribution to the M_{GT} strengths. The calculated M_{GT} values also seem to be sensitive to the κ_f value, in such a way that, as $|\kappa_f|$ decreases, the GT strengths look more densely populated in the lower energy region of $E_x(1_1^+)$, and are also more fragmented. For the $^{98}\text{Zr}(0_1^+) \rightarrow ^{98}\text{Nb}(1_1^+)$ decay, the corresponding M_{GT} distribution pattern with $\kappa_f = -0.780$ MeV more or less resembles the one obtained with $\kappa_f = -0.405$ MeV, since in both cases the total M_{GT} sum would

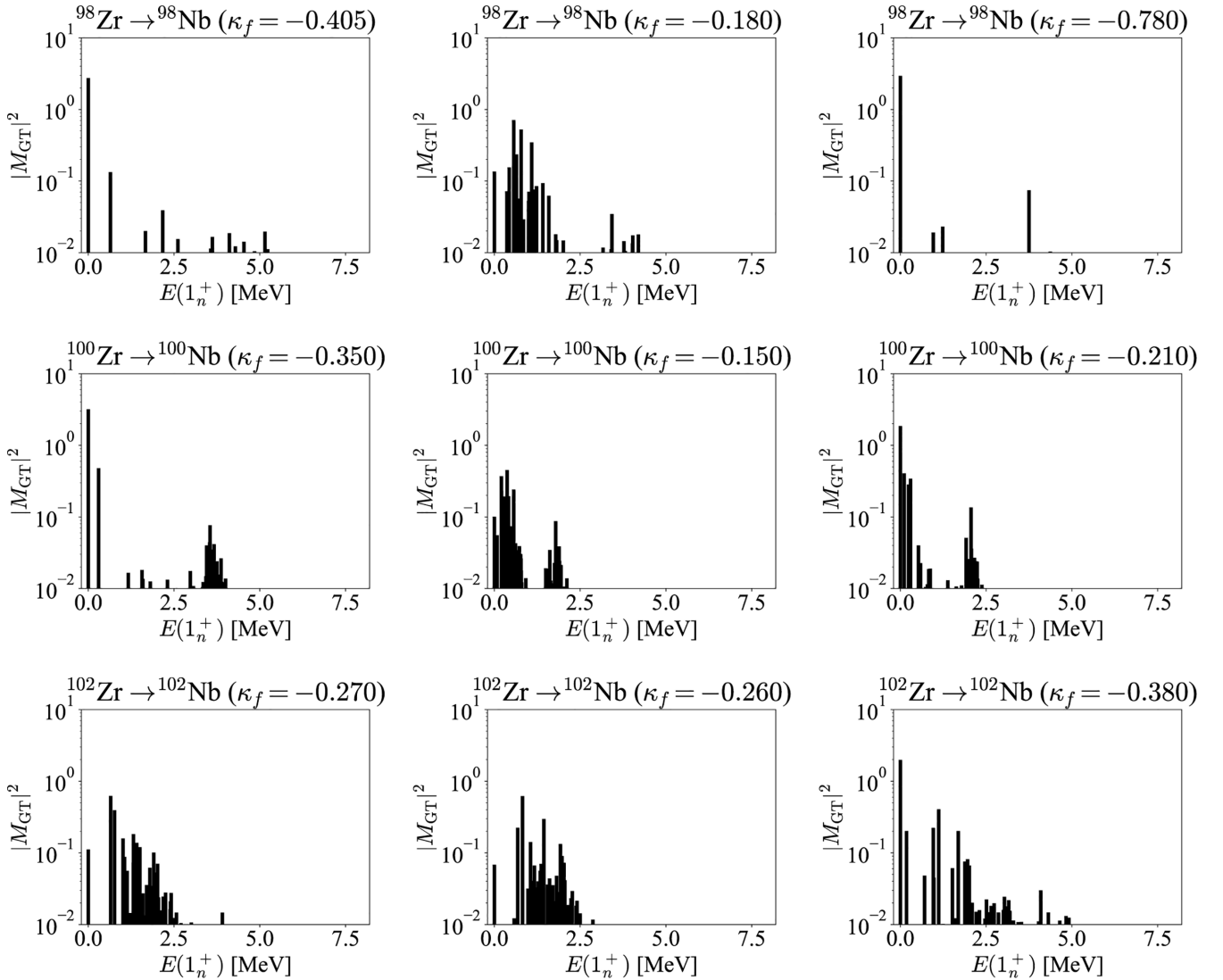


FIG. 7. Absolute squares of the calculated GT transition matrix elements, $|M_{GT}|^2$, for the $^{98,100,102}\text{Zr}(0_1^+) \rightarrow ^{98,100,102}\text{Nb}(1^+)$ transitions as functions of the excitation energies $E_x(1_n^+)$ of all the 1^+ states, obtained from the IBFFM-2 that employs the κ_f values (shown in MeV units) that have been determined from the RHB-to-IBM mapping procedure [35] (left column), and that are obtained in the present study so as to give a reasonable agreement with the experimental $\log_{10} ft(0_1^+ \rightarrow 1_1^+)$ value (middle column). On the right column shown are the results using those κ_f value that correspond to a “spike” pattern in the calculated $\log_{10} ft$ value. See the main text for details.

be mainly accounted for by the GT transition to the lowest energy 1^+ state. The overall patterns of the GT strengths for the $^{100}\text{Zr}(0_1^+) \rightarrow ^{100}\text{Nb}(1^+)$ decay are qualitatively similar between the calculations employing the three different values of κ_f , in that mainly two peaks appear below $E_x(1^+) \approx 1$ MeV, and near or above $E_x(1^+) \approx 1$ MeV. Regarding the $^{102}\text{Zr}(0_1^+) \rightarrow ^{102}\text{Nb}(1^+)$ β^- decay, the systematic behaviors of the M_{GT} distributions with different κ_f values are similar to each other, as well.

In Fig. 8 we show running sums of the GT transition strengths $\sum_n |M_{GT}(0_1^+ \rightarrow 1_n^+)|^2$ for the $^{98,100,102}\text{Zr}(0_1^+) \rightarrow ^{98,100,102}\text{Nb}(1^+)\beta^-$ decays with respect to $E_x(1^+)$, calculated with three different values of the parameter κ_f . For all the transitions shown in the figure, one can observe a systematic trend that, for larger $|\kappa_f|$ the GT running sum is mostly

accounted for by the transitions to lowest-lying 1^+ states. This is also confirmed from the $|M_{GT}|^2$ systematic in Fig. 7. For the $^{98}\text{Zr}(0_1^+) \rightarrow ^{98}\text{Nb}(1^+)$ decay, $\sum_n |M_{GT}|^2$ with $\kappa_f = -0.405$ and -0.780 MeV are shown to be converged already near the lowest energy, 1_1^+ state. In the case of $\kappa_f = -0.180$ MeV, on the other hand, contributions from the lowest 1^+ states are negligible. The sum rises at $E_x(1^+) \approx 1$ MeV, and converges to $\sum_n |M_{GT}|^2 \approx 3$ at $E_x(1^+) \approx 4$ MeV. The calculated GT sums with the three different κ_f 's seem to converge consistently to $\sum_n |M_{GT}|^2 \approx 3$, meaning that the GT sum does not depend much on the parameter κ_f for the $^{98}\text{Zr}(0_1^+) \rightarrow ^{98}\text{Nb}(1^+)$ decay.

This finding appears to be rather at variance with the results for the $^{100,102}\text{Zr}(0_1^+) \rightarrow ^{100,102}\text{Nb}(1^+)$ decays. In these cases, as we decrease $|\kappa_f|$, the running sum $\sum_n |M_{GT}|^2$

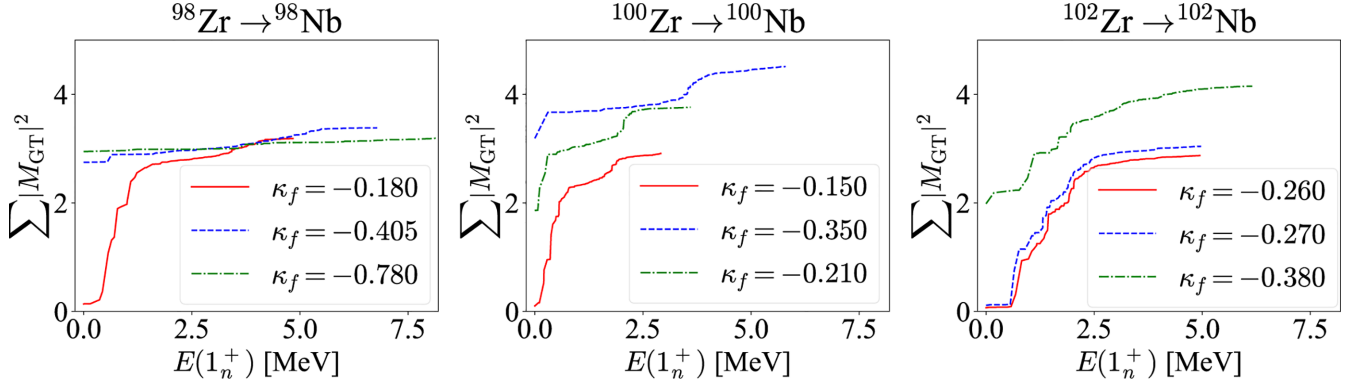


FIG. 8. Running sums, $|M_{GT}|^2$, as functions of the excitation energies $E_x(1_n^+)$ for all the 1^+ states of the odd-odd $^{98,100,102}\text{Nb}$ nuclei, that are obtained from the IBFFM-2 Hamiltonian, using the optimal κ_f parameter (shown in MeV units) with which the experimental $\log_{10} ft(0_1^+ \rightarrow 1_1^+)$ value is reproduced (solid curves) and the one determined by the mapping procedure [35] (dashed lines). The results in the case of the κ_f value that gives the spike-like pattern in the calculated $\log_{10} ft$ values are also depicted as dashed-dotted curves.

converges at low $E_x(1^+)$ energies, and the converged value becomes smaller, e.g., $\sum_n |M_{GT}|^2 \approx 4.5, 3.7,$ and 2.8 for the $^{100}\text{Zr}(0_1^+) \rightarrow ^{100}\text{Nb}(1^+)$ decay with $\kappa_f = -0.350, -0.210,$ and -0.150 MeV, respectively. The variation of κ_f is, therefore, shown to affect much the $\sum_n |M_{GT}|^2$ sums, as regards the $^{100,102}\text{Zr}(0_1^+) \rightarrow ^{100,102}\text{Nb}(1^+)$ decays.

IV. IMPACTS ON THE ENERGY SPECTRA

We now turn to discuss the parameter dependence of the results on the low-lying states of each nucleus involved, specifically focusing on the energy levels of the odd-odd Nb nuclei. Given the fact that among all the model parameters involved in the $\log_{10} ft$ calculations, the strength parameters κ_f and v_t most affect the $\log_{10} ft(0_1^+ \rightarrow 1_1^+)$ predictions (cf. Figs. 2 and 5), we analyze in particular the behaviors of low-spin yrast states of the odd-odd Nb nuclei when these parameters are varied simultaneously. We show in Fig. 9 contour plots of the calculated $1_1^+, 2_1^+, 3_1^+, 4_1^+, 5_1^+,$ and 6_1^+ states of the odd-odd $^{96-102}\text{Nb}$ nuclei in terms of the parameters κ_f and v_t . In each plot, those (κ_f, v_t) values giving the excitation energies that agree with the available experimental data are connected by the dashed lines.

As mentioned earlier, the measured ground state of ^{96}Nb has the spin and parity $I^\pi = 6^+$ [50]. One sees in Fig. 9 that the 5_1^+ and 6_1^+ excitation energies of ^{96}Nb are sensitive to κ_f within the range $\kappa_f \gtrsim -0.2$, and to v_t with its value being near $v_t = 0$ MeV. Optimal (κ_f, v_t) values that are to reproduce the correct 6^+ ground-state spin should also be extracted somewhere from these parameter ranges.

As is shown in Fig. 6, overall behaviors of the excitation energies within the (κ_f, v_t) plane look similar between ^{98}Nb and ^{100}Nb , which are, however, rather different from the one for the ^{102}Nb nucleus. The calculated energies for the heavier Nb nuclei, $^{98-102}\text{Nb}$, appear to depend on these parameters more strongly than in the case of ^{96}Nb , e.g., for the 5_1^+ and 6_1^+ states. The ground state for $^{98,100,102}\text{Nb}$ is experimentally suggested to be the 1^+ state. As one sees from the behaviors of the dashed curves in Fig. 9, v_t should take a positive value so that the measured ground-state spin should be reproduced

correctly. Given a positive v_t value, then typical κ_f values that reproduce the excitation energies of the states other than 1_1^+ may be, perhaps, within the range $-0.3 \gtrsim \kappa_f \gtrsim -0.2$ MeV, in which the energies significantly depend on κ_f . It is, however, not very obvious to find a best set of the (κ_f, v_t) values that reproduces all the excitation energies, as well as the observed $\log_{10} ft(0_1^+ \rightarrow 1_1^+)$ values satisfactorily. Other model parameters, e.g., those for the spin-spin- δ and spin-spin interactions for the residual neutron-proton correlations, may need to be taken into account as other adjustable parameters. Such an analysis would invoke further complications, and is beyond the scope of the present study.

To shed light upon the search for optimal sets of the (κ_f, v_t) parameters, we now consider as constraints the $\log_{10} ft(0_1^+ \rightarrow 1_1^+)$ data, and the ground-state spin of 1^+ for the odd-odd $^{98,100,102}\text{Nb}$ nuclei. Figure 10 indicates regions of those values of the parameters κ_f and v_t , shown as shaded areas, that give the 1_1^+ state to be the ground state of the odd-odd final nuclei for the $0_1^+ \rightarrow 1_1^+$ GT transitions of the $^{98}\text{Zr}, ^{100}\text{Zr},$ and ^{102}Zr nuclei. Also indicated in Fig. 10 are those (κ_f, v_t) values, which are connected by solid curves, that reproduce the observed $\log_{10} ft$ value for each of the $^A\text{Zr}(0_1^+) \rightarrow ^A\text{Nb}(1_1^+) \beta^-$ decays. Optimal sets of the (κ_f, v_t) values would be those at which the $\log_{10} ft$ curve passes through the shaded area in the figure. They could be $0.1 \lesssim v_t \lesssim 0.5$ MeV and $-0.15 \lesssim \kappa_f \lesssim -0.25$ MeV for ^{98}Nb , and $v_t \gtrsim 0.2$ MeV and $\kappa_f \gtrsim -0.15$ MeV for ^{100}Nb . As for ^{102}Nb , there are basically two regions in which the crossing of the $\log_{10} ft$ curve across the shaded area is visible: one with $0 \lesssim v_t \lesssim 0.15$ MeV and $-0.5 \lesssim \kappa_f \lesssim -0.4$ MeV, and the other with $v_t \gtrsim 0.25$ MeV and $\kappa_f \gtrsim -0.25$ MeV. The aforementioned κ_f values, i.e., $\kappa_f = -0.180, -0.150,$ and -0.260 MeV, and $v_t = 0.28, 0.50,$ and 0.50 MeV for $^{98,100,102}\text{Nb}$, respectively, leading to a good agreement with the $\log_{10} ft(0_1^+ \rightarrow 1_1^+)$ data, more or less fall into these ranges.

Figure 11 shows the calculated low-energy levels for the odd-odd $^{98,100,102}\text{Nb}$ nuclei employing those parameters derived from the RHB-to-IBM mapping in Ref. [35], and the optimal κ_f parameter that gives reasonable agreement with the $\log_{10} ft(0_1^+ \rightarrow 1_1^+)$ data for the $^A\text{Zr} \rightarrow ^A\text{Nb} \beta^-$ decay:

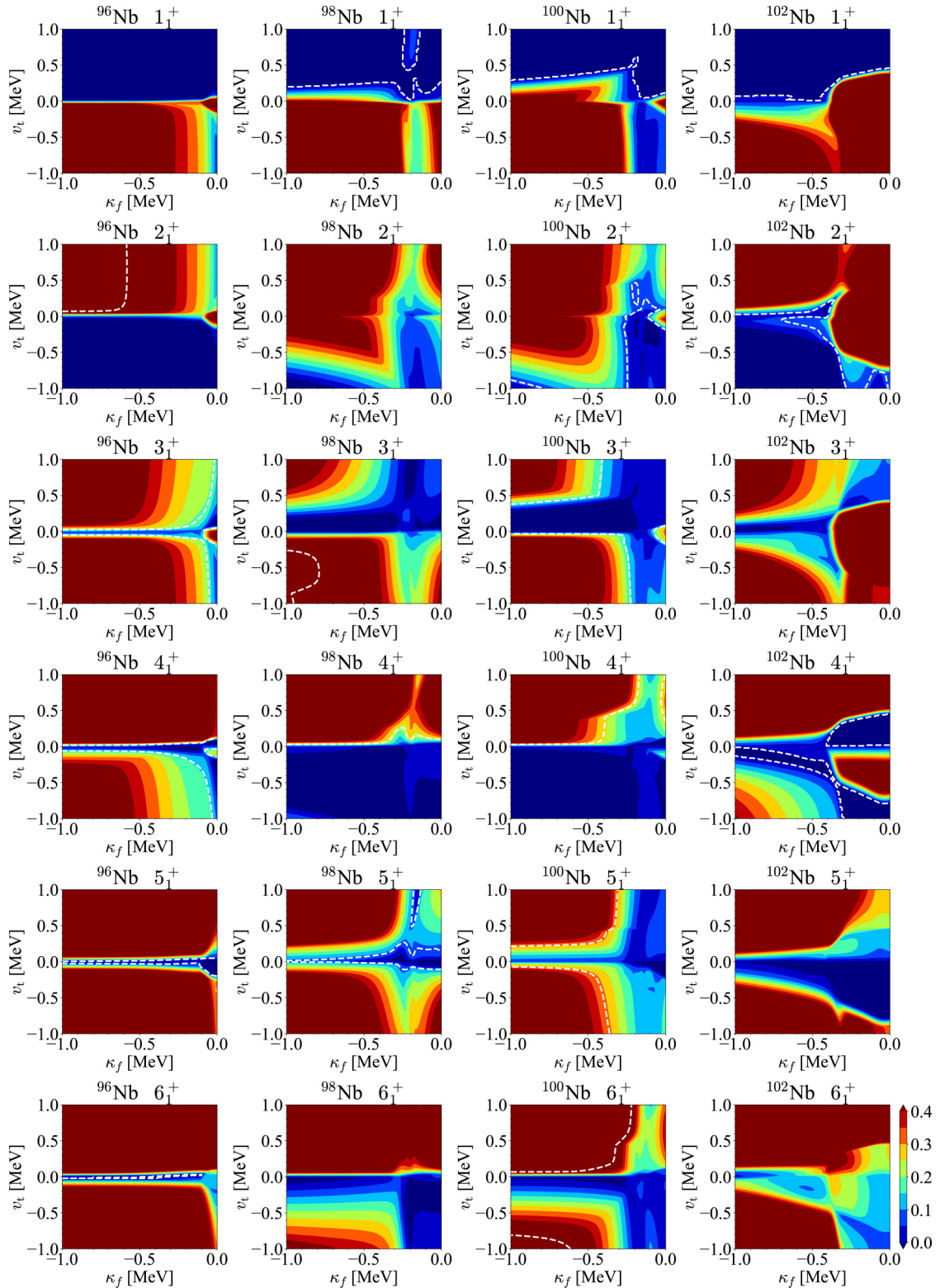


FIG. 9. Contour plots of the calculated excitation energies for the yrast 1^+ , 2^+ , 3^+ , 4^+ , 5^+ , and 6^+ states of the daughter nuclei Nb shown as functions of the parameters κ_f and v_t used for the odd-odd Nb nuclei. The dashed lines in each panel connect values corresponding to the experimental excitation energies.

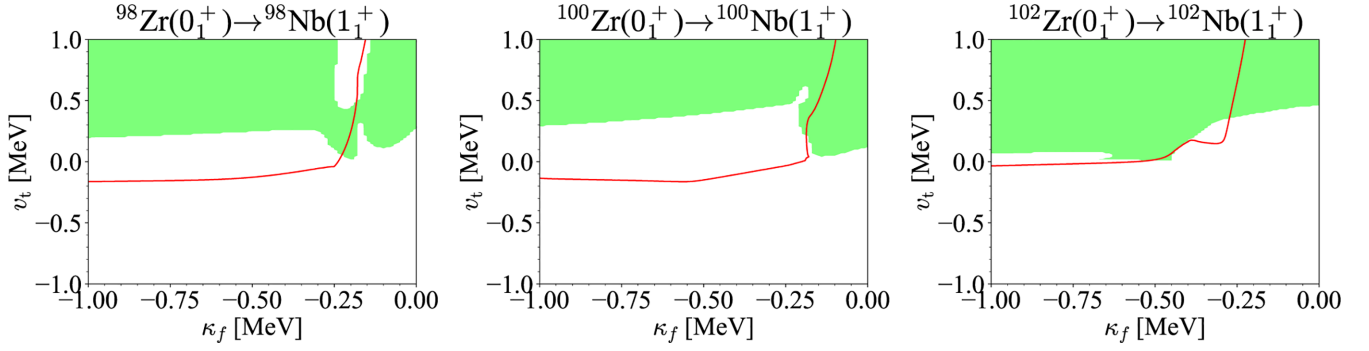


FIG. 10. Regions of those κ_f and v_t parameters (shaded areas) that give the 1_1^+ state to be the ground state for $^{98,100,102}\text{Nb}$. The solid curves connect the (κ_f, v_t) values with which the experimental $\log_{10} ft(0_1^+ \rightarrow 1_1^+)$ values for the $\text{Zr} \rightarrow \text{Nb} \beta^-$ decay [50] are reproduced.

$\kappa_f = -0.180$, -0.150 , and -0.260 MeV, for $A = 98$, 100 , and 102 , respectively. All the other model parameters, including v_t , are the same as those used for the mapped IBM-2 calculations (see Table III). The corresponding experimental energy spectrum [50] is also included. An overall effect of using the optimal κ_f strength parameter for $^{98,100}\text{Nb}$ is to compress the energy spectrum. For ^{98}Nb , the energy levels for the 4_1^+ and 5_1^+ states are lowered in the present IBFFM-2 calculation, and agree with the experimental data better than the previous calculation in Ref. [35]. The 3_1^+ energy level is calculated to be very near the 1_1^+ ground state in both versions of the IBFFM-2. It is quite at variance with experiment, which rather suggests this state to be found at the excitation energy of 737 keV. We note that for ^{98}Nb spins for all the observed levels included in Fig. 11, but for the 1^+ one, have not been firmly established experimentally. The energy spectrum for the ^{100}Nb obtained in the present work is even more compressed with respect to the one in the previous study [35]. An improvement over the previous mapped-IBM-2 calculation is only seen in the energy level of the 2_1^+ state, which agrees with data. The spins and parities of those states other than the 1^+ ground state have not been established for ^{100}Nb , either. For ^{102}Nb , the energy spectra resulting from the mapped IBM-2 and the present calculation look strikingly similar to each other. This reflects the fact that the mapped IBM-2 calculation in Ref. [35] already reproduced satisfactorily the $\log_{10} ft(0_1^+ \rightarrow 1_1^+)$ value for the $^{102}\text{Zr} \rightarrow ^{102}\text{Nb}$ decay, and the κ_f parameter employed

there ($\kappa_f = -0.270$ MeV) is close to that optimal value extracted in the present study. Determination of the spin and parity of ^{102}Nb has been under debate, and is only tentatively assigned to be 4^+ in the NNDC database. But since the lowest energy state for which the spin and parity are identified is the 1^+ state, we here regard the 1^+ state as the ground state of ^{102}Nb .

In Fig. 12, we make similar comparisons to those in Fig. 11 for the IBM-2 energy spectra for the even-even $^{98,100,102}\text{Mo}$ nuclei, since they are used as the even-even boson cores for the odd-odd $^{98,100,102}\text{Nb}$ nuclei, respectively. Just as in the cases of the odd-odd Nb nuclei, a notable effect of using the optimal κ_f parameter in the present analysis is to compress the whole energy spectrum with respect to the previous mapped IBM-2 calculations for ^{98}Mo and ^{100}Mo . As for ^{102}Mo , there is essentially no difference between the two IBM-2 calculations, since the employed κ_f values are similar. In general, the new calculations reproduce the experimental energy spectra better than the previous ones for $^{98,100}\text{Mo}$.

We note that, within the mapped IBM-2 framework, the derived quadrupole-quadrupole strength parameter between unlike bosons is shown to be generally so large in magnitude that the resulting energy spectra, especially for those of the non-yrast states, are predicted to be considerably higher than the experimental ones. We might then attribute the too large derived quadrupole-quadrupole boson interaction strength to the properties of the EDF and/or the pairing properties

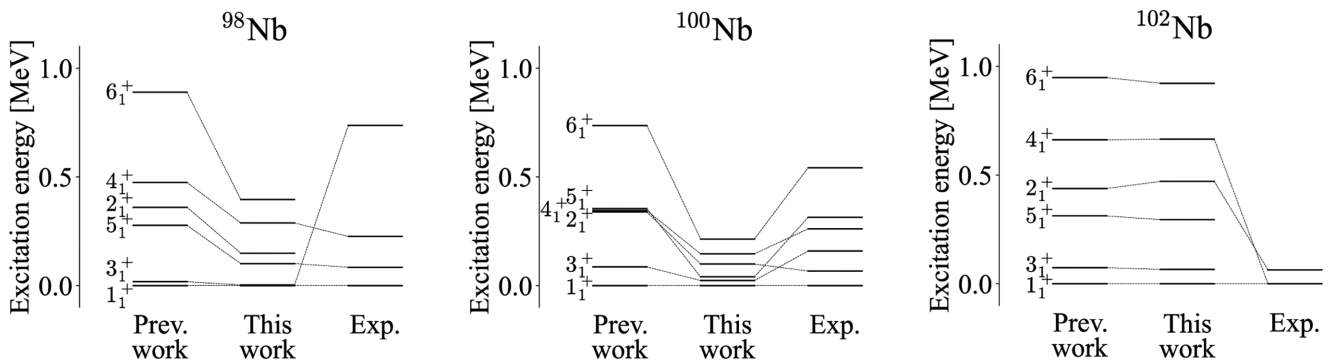


FIG. 11. Comparison of the low-energy spectra for the odd-odd $^{98,100,102}\text{Nb}$ nuclei calculated with the parameters that give a reasonable agreement with the experimental $\log_{10} ft(0_1^+ \rightarrow 1_1^+)$ data to those obtained in Ref. [35], and to the experimental data [50].

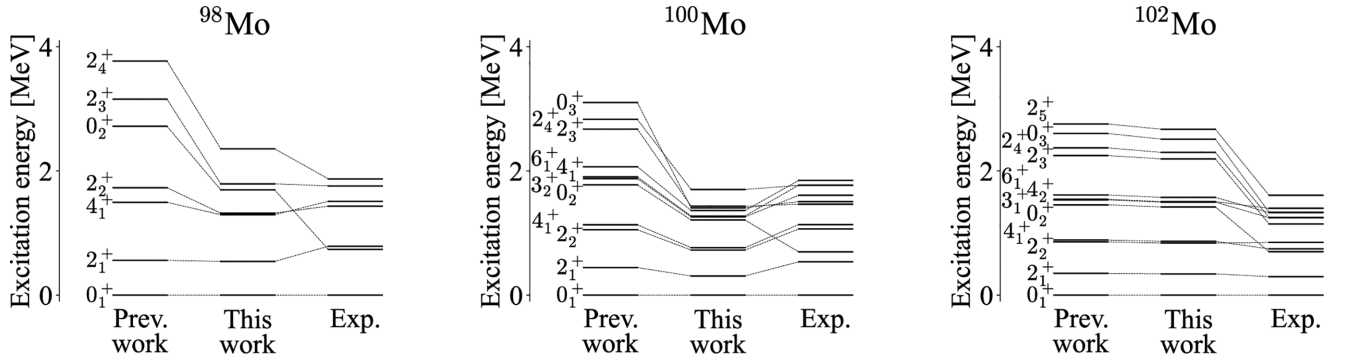


FIG. 12. Same as Fig. 11, but for the energy spectra for the even-even $^{98,100,102}\text{Mo}$ nuclei.

employed in the SCMF calculations, upon which the mapping procedure is based. One immediate solution would be to adjust some of the parameters in the EDF-SCMF model so as to provide a reliable microscopic input to the IBM-2 that leads to an improved description of the low-lying states and β -decay properties simultaneously. By increasing the strength of the pairing correlations, for instance, the SCMF calculations yield the PESs that are softer in deformation variables, and the derived quadrupole-quadrupole strength in the IBM-2 Hamiltonian is expected to be smaller than otherwise, thus leading to a better description of the measured low-lying states as well as the β -decay properties.

It should be also noted that, for all these three Mo isotopes near $N = 60$, the roles of shape coexistence and intruder excitations are expected to be significant [43,51–54], which is indeed reflected in the low-lying 0_2^+ energy level found in the vicinity of the 2_1^+ one. The low-lying 0_2^+ levels could not be reproduced by the version of the IBM-2, that is adopted here and in Ref. [35]. The low-lying 0^+ states and shape coexistence could be handled within the IBM, e.g., by incorporating effects of configuration mixing between normal and intruder states [55], as was considered in previous mapped IBM calculations [53,56].

V. SUMMARY AND CONCLUSIONS

We have analyzed the parameter dependence of the calculated β -decay properties, as well as the low-lying states, of the neutron-rich Zr isotopes within the IBM-2 and IBFFM-2. The present analysis is a continuation of the preceding IBM-2 study on the β -decay properties in this mass region, which was based on the microscopic EDF framework. The present study aims to identify which of the various model parameters affect most the predictions on β decay and also play a key role in improving the accuracy in reproducing the experimental data. The calculated $\log_{10} ft$ values for the β^- decays of the neutron-rich even-even $^{96-102}\text{Zr}$ into odd-odd $^{96-102}\text{Nb}$ nuclei here have been shown to exhibit consistently strong dependencies on the model parameters that are associated with the quadrupole-quadrupole interaction strength (κ_f), and with the residual neutron-proton interaction of tensor type (v_t), which

are involved in the IBFFM-2 Hamiltonian for describing the odd-odd daughter Nb nuclei. Along with the $\log_{10} ft$ values, we have also investigated the parameter dependencies of the calculated excitation energies for the low-spin and low-lying states for the odd-odd Nb nuclei, and the GT strength distributions.

The problem encountered in the previous mapped IBM-2 calculations [35] was that the measured β^- -decay $\log_{10} ft(0_1^+ \rightarrow 1_1^+)$ values for the ^{98}Zr and ^{100}Zr nuclei in particular were underestimated by a factor of ≈ 1.5 . The analyses made in the present study have indicated that a major cause of this discrepancy is the fact that the κ_f parameter obtained by the mapping procedure might have been too large in magnitude. It has been indeed shown here that reductions in magnitude of κ_f by approximately a factor of 2 would be required to improve the mapped-IBM-2 description of $\log_{10} ft(0_1^+ \rightarrow 1_1^+)$ values. The reduced $|\kappa_f|$ value leading to a good agreement with the measured $\log_{10} ft(0_1^+ \rightarrow 1_1^+)$ has been, in turn, employed for calculating the low-lying states of each nucleus, and it has been shown that the reduction of $|\kappa_f|$ improves significantly the description of the low-lying energy levels for the even-even $^{98,100}\text{Mo}$ nuclei, which are considered as the boson cores for the odd-odd $^{98,100}\text{Nb}$ nuclei, respectively.

The fact that the too large quadrupole-quadrupole interaction strength for the even-even nuclei was obtained in the mapped IBM-2 could be partly attributed to the properties of the EDF-SCMF calculations. Possible impacts of the parameters involved in the EDF calculations, e.g., pairing strengths, on the spectroscopic properties and fundamental nuclear processes, such as the single- β and double- β decays, could be investigated as a further step for a precise IBM description. In addition, as the present analysis was focused specifically on the Zr isotopes, it could be extended further to other nuclear systems. We could also take into account additional parameters in the IBM-2 and IBFFM-2 Hamiltonians that could have influences on the $\log_{10} ft$ predictions, including the single-particle energies, and occupation probabilities. Sensitivities of the calculated quantities would be then analyzed in a larger parameter space. The work along these lines is in progress, and will be reported elsewhere.

- [1] I. Dillmann, K.-L. Kratz, A. Wöhr, O. Arndt, B. A. Brown, P. Hoff, M. Hjorth-Jensen, U. Köster, A. N. Ostrowski, B. Pfeiffer, D. Seweryniak, J. Shergur, and W. B. Walters (ISOLDE Collaboration), *Phys. Rev. Lett.* **91**, 162503 (2003).
- [2] S. Nishimura, Z. Li, H. Watanabe, K. Yoshinaga, T. Sumikama, T. Tachibana, K. Yamaguchi, M. Kurata-Nishimura, G. Lorusso, Y. Miyashita, A. Odahara, H. Baba, J. S. Berryman, N. Blasi, A. Bracco, F. Camera, J. Chiba, P. Doornenbal, S. Go, T. Hashimoto *et al.*, *Phys. Rev. Lett.* **106**, 052502 (2011).
- [3] M. Quinn, A. Aprahamian, J. Pereira, R. Surman, O. Arndt, T. Baumann, A. Becerril, T. Elliot, A. Estrade, D. Galaviz, T. Ginter, M. Hausmann, S. Hennrich, R. Kessler, K.-L. Kratz, G. Lorusso, P. F. Mantica, M. Matos, F. Montes, B. Pfeiffer *et al.*, *Phys. Rev. C* **85**, 035807 (2012).
- [4] G. Lorusso, S. Nishimura, Z. Y. Xu, A. Jungclaus, Y. Shimizu, G. S. Simpson, P.-A. Söderström, H. Watanabe, F. Browne, P. Doornenbal, G. Gey, H. S. Jung, B. Meyer, T. Sumikama, J. Taprogge, Z. Vajta, J. Wu, H. Baba, G. Benzoni, K. Y. Chae *et al.*, *Phys. Rev. Lett.* **114**, 192501 (2015).
- [5] R. Caballero-Folch, C. Domingo-Pardo, J. Agramunt, A. Algora, F. Ameil, A. Arcones, Y. Ayyad, J. Benlliure, I. N. Borzov, M. Bowry, F. Calviño, D. Cano-Ott, G. Cortés, T. Davinson, I. Dillmann, A. Estrade, A. Evdokimov, T. Faestermann, F. Farinon, D. Galaviz *et al.*, *Phys. Rev. Lett.* **117**, 012501 (2016).
- [6] F. T. Avignone, S. R. Elliott, and J. Engel, *Rev. Mod. Phys.* **80**, 481 (2008).
- [7] J. Engel and J. Menéndez, *Rep. Prog. Phys.* **80**, 046301 (2017).
- [8] M. Agostini, G. Benato, J. A. Detwiler, J. Menéndez, and F. Vissani, *Rev. Mod. Phys.* **95**, 025002 (2023).
- [9] K. Langanke and G. Martínez-Pinedo, *Rev. Mod. Phys.* **75**, 819 (2003).
- [10] E. Caurier, G. Martínez-Pinedo, F. Nowack, A. Poves, and A. P. Zuker, *Rev. Mod. Phys.* **77**, 427 (2005).
- [11] S. Yoshida, Y. Utsuno, N. Shimizu, and T. Otsuka, *Phys. Rev. C* **97**, 054321 (2018).
- [12] T. Suzuki, S. Shibagaki, T. Yoshida, T. Kajino, and T. Otsuka, *Astrophys. J.* **859**, 133 (2018).
- [13] R. Álvarez-Rodríguez, P. Sarriguren, E. Moya de Guerra, L. Paceaescu, A. Faessler, and F. Šimkovic, *Phys. Rev. C* **70**, 064309 (2004).
- [14] P. Sarriguren, *Phys. Rev. C* **91**, 044304 (2015).
- [15] J. M. Boillos and P. Sarriguren, *Phys. Rev. C* **91**, 034311 (2015).
- [16] P. Pirinen and J. Suhonen, *Phys. Rev. C* **91**, 054309 (2015).
- [17] F. Šimkovic, V. Rodin, A. Faessler, and P. Vogel, *Phys. Rev. C* **87**, 045501 (2013).
- [18] M. T. Mustonen and J. Engel, *Phys. Rev. C* **93**, 014304 (2016).
- [19] J. T. Suhonen, *Front. Phys.* **5**, 55 (2017).
- [20] A. Ravlić, E. Yüksel, Y. F. Niu, and N. Paar, *Phys. Rev. C* **104**, 054318 (2021).
- [21] K. Yoshida, Y. Niu, and F. Minato, *Phys. Rev. C* **108**, 034305 (2023).
- [22] P. Navrátil and J. Dobe, *Phys. Rev. C* **37**, 2126 (1988).
- [23] F. Dellagiacoma, Beta decay of odd mass nuclei in the interacting boson-fermion model, Ph.D. thesis, Yale University, 1988.
- [24] F. Dellagiacoma and F. Iachello, *Phys. Lett. B* **218**, 399 (1989).
- [25] S. Brant, N. Yoshida, and L. Zuffi, *Phys. Rev. C* **70**, 054301 (2004).
- [26] S. Brant, N. Yoshida, and L. Zuffi, *Phys. Rev. C* **74**, 024303 (2006).
- [27] N. Yoshida and F. Iachello, *Prog. Theor. Exp. Phys.* **2013**, 043D01.
- [28] E. Mardones, J. Barea, C. E. Alonso, and J. M. Arias, *Phys. Rev. C* **93**, 034332 (2016).
- [29] K. Nomura, R. Rodríguez-Guzmán, and L. M. Robledo, *Phys. Rev. C* **101**, 024311 (2020).
- [30] K. Nomura, R. Rodríguez-Guzmán, and L. M. Robledo, *Phys. Rev. C* **101**, 044318 (2020).
- [31] J. Ferretti, J. Kotila, R. I. M. Vsevolodovna, and E. Santopinto, *Phys. Rev. C* **102**, 054329 (2020).
- [32] K. Nomura, *Phys. Rev. C* **105**, 044306 (2022).
- [33] K. Nomura, L. Lotina, R. Rodríguez-Guzmán, and L. M. Robledo, *Phys. Rev. C* **106**, 064304 (2022).
- [34] R. I. Magaña Vsevolodovna, E. Santopinto, and R. Bijker, *Phys. Rev. C* **106**, 044307 (2022).
- [35] K. Nomura, *Phys. Rev. C* **109**, 034319 (2024).
- [36] D. Vretenar, A. V. Afanasjev, G. A. Lalazissis, and P. Ring, *Phys. Rep.* **409**, 101 (2005).
- [37] T. Nikšić, D. Vretenar, and P. Ring, *Prog. Part. Nucl. Phys.* **66**, 519 (2011).
- [38] T. Nikšić, D. Vretenar, and P. Ring, *Phys. Rev. C* **78**, 034318 (2008).
- [39] Y. Tian, Z. Y. Ma, and P. Ring, *Phys. Lett. B* **676**, 44 (2009).
- [40] J. N. Ginocchio and M. W. Kirson, *Nucl. Phys. A* **350**, 31 (1980).
- [41] S. Brant, V. Paar, and D. Vretenar, *Z. Phys. A* **319**, 355 (1984).
- [42] F. Iachello and P. Van Isacker, *The Interacting Boson-Fermion Model* (Cambridge University Press, Cambridge, 1991).
- [43] K. Heyde and J. L. Wood, *Rev. Mod. Phys.* **83**, 1467 (2011).
- [44] F. Iachello and A. Arima, *The Interacting Boson Model* (Cambridge University Press, Cambridge, 1987).
- [45] T. Otsuka, A. Arima, F. Iachello, and I. Talmi, *Phys. Lett. B* **76**, 139 (1978).
- [46] T. Otsuka, A. Arima, and F. Iachello, *Nucl. Phys. A* **309**, 1 (1978).
- [47] O. Scholten, *Prog. Part. Nucl. Phys.* **14**, 189 (1985).
- [48] T. Mizusaki and T. Otsuka, *Prog. Theor. Phys. Suppl.* **125**, 97 (1996).
- [49] K. Nomura, N. Shimizu, and T. Otsuka, *Phys. Rev. Lett.* **101**, 142501 (2008).
- [50] Brookhaven National Nuclear Data Center, <http://www.nndc.bnl.gov>.
- [51] T. Thomas, K. Nomura, V. Werner, T. Ahn, N. Cooper, H. Duckwitz, M. Hinton, G. Ilie, J. Jolie, P. Petkov, and D. Radeck, *Phys. Rev. C* **88**, 044305 (2013).
- [52] T. Thomas, V. Werner, J. Jolie, K. Nomura, T. Ahn, N. Cooper, H. Duckwitz, A. Fitzler, C. Fransen, A. Gade, M. Hinton, G. Ilie, K. Jessen, A. Linnemann, P. Petkov, N. Pietralla, and D. Radeck, *Nucl. Phys. A* **947**, 203 (2016).
- [53] K. Nomura, R. Rodríguez-Guzmán, and L. M. Robledo, *Phys. Rev. C* **94**, 044314 (2016).
- [54] P. E. Garrett, M. Zielnińska, and E. Clément, *Prog. Part. Nucl. Phys.* **124**, 103931 (2022).
- [55] P. D. Duval and B. R. Barrett, *Phys. Lett. B* **100**, 223 (1981).
- [56] K. Nomura, R. Rodríguez-Guzmán, L. M. Robledo, and N. Shimizu, *Phys. Rev. C* **86**, 034322 (2012).